



# CHORUS

This is the accepted manuscript made available via CHORUS. The article has been published as:

## Kardar-Parisi-Zhang Interfaces with Curved Initial Shapes and Variational Formula

Yohsuke T. Fukai and Kazumasa A. Takeuchi

Phys. Rev. Lett. **124**, 060601 — Published 10 February 2020

DOI: [10.1103/PhysRevLett.124.060601](https://doi.org/10.1103/PhysRevLett.124.060601)

# 1 Kardar-Parisi-Zhang Interfaces with Curved Initial Shapes and Variational Formula

2 Yohsuke T. Fukai<sup>1,2,\*</sup> and Kazumasa A. Takeuchi<sup>2,†</sup>

3 <sup>1</sup>*RIKEN Center for Biosystems Dynamics Research*

4 <sup>2</sup>*Department of Physics, the University of Tokyo*

5 (Dated: January 8, 2020)

We study fluctuations of interfaces in the Kardar-Parisi-Zhang (KPZ) universality class with curved initial conditions. By simulations of a cluster growth model and experiments of liquid-crystal turbulence, we determine the universal scaling functions that describe the height distribution and the spatial correlation of the interfaces growing outward from a ring. The scaling functions, controlled by a single dimensionless time parameter, show crossover from the statistical properties of the flat interfaces to those of the circular interfaces. Moreover, employing the KPZ variational formula to describe the case of the ring initial condition, we find that the formula, which we numerically evaluate, reproduces the numerical and experimental results precisely without adjustable parameters. This demonstrates that precise numerical evaluation of the variational formula is possible at all, and underlines the practical importance of the formula, which is able to predict the one-point distribution of KPZ interfaces for general initial conditions.

6 Efforts on universal behavior associated with scale in-  
7 variance, which have established important concepts such  
8 as the renormalization group and the universality class,  
9 now shed light on novel aspects of nonequilibrium fluctua-  
10 tions. In this respect, the Kardar-Parisi-Zhang (KPZ)  
11 universality class [1–4] plays a distinguished role, because  
12 of the existence of exact solutions and experimental real-  
13 izations. The KPZ class is also known to arise in a vari-  
14 ety of problems: besides growing interfaces and directed  
15 polymers as originally proposed [1], it also turned out  
16 to be relevant for stochastic particle transport, quantum  
17 integrable systems [3, 4], and fluctuating hydrodynamics  
18 [5], to name but a few.

19 In the following, let us focus on the one-dimensional  
20 case, for which exact studies have been developed,  
21 and consider growing interfaces described by the height  
22  $h(x, t)$  at position  $x \in \mathbb{R}$  and time  $t \in \mathbb{R}$ . The KPZ  
23 class describes scale-invariant fluctuations of growing in-  
24 terfaces in the long-time limit, in general situations with-  
25 out particular symmetries and conservation laws. The  
26 hallmark of the KPZ class is the scaling laws for the  
27 fluctuation amplitude  $\sim t^\beta$  and the correlation length  
28  $\sim t^{1/z}$ , with universal exponents  $\beta$  and  $z$  that take the  
29 values  $\beta = 1/3$  and  $z = 3/2$  for the one-dimensional case  
30 [1, 2, 4]. The height  $h(x, t)$  is then generally written, for  
31 large  $t$ , as

$$h(x, t) \simeq v_\infty t + (\Gamma t)^{1/3} \chi(X, t) \quad (1)$$

32 where  $\chi(X, t)$  is a stochastic variable,  $X := x/\xi(t)$  de-  
33 notes the coordinate rescaled by the correlation length  
34  $\xi(t) := \frac{2}{A} (\Gamma t)^{2/3}$ , and  $v_\infty, \Gamma, A$  are system-dependent pa-  
35 rameters. The variable  $\chi(X, t)$  is expected to be univer-  
36 sal, in the sense that its statistical properties do not de-  
37 pend on microscopic details of the systems. The scaling  
38 exponents of the KPZ class have been found in various  
39 experimental systems [6], including colonies of living cells  
40 [7, 8], combusting paper [9], and liquid-crystal turbulence  
41 [4, 10–12].

42 Recently, remarkable developments triggered by exact  
43 studies [3, 4] have unveiled novel aspects on the KPZ  
44 class. A particularly important outcome is the geome-  
45 try dependence, which we describe below. If an inter-  
46 face grows on top of a flat substrate, as usually assumed  
47 in simulations, the interface roughens but maintains the  
48 globally flat profile. In contrast, if an interface in a plane  
49 starts to grow from a point nucleus, say, at  $x = 0$ , it takes  
50 a circular shape with a growing radius. Although this in-  
51 terface becomes flatter and flatter as the radius increases,  
52 statistical properties of  $\chi(X, t)$  remain distinct from the  
53 flat case. Specifically,  $\chi(X, t)$  has different asymptotic  
54 behavior as follows

$$\chi(X, t) \xrightarrow{d} \begin{cases} \mathcal{A}_1(X), & \text{(flat)} \\ \mathcal{A}_2(X) - X^2, & \text{(circular)} \end{cases} \quad (2)$$

55 where  $\xrightarrow{d}$  denotes convergence in distribution ( $\stackrel{d}{=}$  and  $\stackrel{d}{\simeq}$   
56 will be used analogously).  $\mathcal{A}_1(X)$  and  $\mathcal{A}_2(X)$  are called  
57 the Airy<sub>1</sub> [13, 14] and Airy<sub>2</sub> [15] processes, respectively,  
58 and well studied analytically [16]. Due to their trans-  
59 lational invariance, as long as one-point properties are  
60 concerned,  $\mathcal{A}_i(X)$  can be replaced by a single stochas-  
61 tic variable  $\chi_i$ . Remarkably, the one-point distribution  
62 of  $\chi_1$  and  $\chi_2$  was shown [17–20] to coincide respectively  
63 with the GOE and GUE Tracy-Widom distribution [21],  
64 known from random matrix theory [22], which describes  
65 the distribution of the largest eigenvalue of random ma-  
66 trices in the Gaussian orthogonal and unitary ensembles  
67 (GOE and GUE). This geometry dependence, as well as  
68 the emergence of the Tracy-Widom distribution, turned  
69 out to be experimentally relevant too, as shown by ex-  
70 periments on liquid-crystal turbulence [4, 10, 11]. Corre-  
71 lation properties were also shown to be different between  
72 the flat and circular cases, even though the scaling ex-  
73 ponents  $\beta$  and  $z$  take the same values. On the basis  
74 of those results, one may state that the flat and circu-  
75 lar interfaces constitute different *universality subclasses*

76 within the single KPZ class, characterized by different  
77 yet universal distribution and correlation properties.

78 Those universality subclasses have been, however,  
79 mostly studied for a few “canonical” cases including the  
80 flat and circular ones. A natural and important question  
81 is then what happens for more general initial conditions.  
82 Theoretically, the *KPZ fixed-point variational formula*  
83 [16, 23–26] can be used to predict the asymptotic proper-  
84 ties of  $\chi(X, t \rightarrow \infty)$  for general initial conditions. On the  
85 other hand, experimental and numerical studies have fo-  
86 cused on finite-time behavior emerging from intermediate  
87 initial conditions. For example, the present authors [12]  
88 studied growth from a ring of finite radius  $R_0$ , which then  
89 produces two curved interfaces, one growing outward and  
90 the other one inward. Focusing on the ingrowing inter-  
91 faces, we found that finite-time properties of  $\chi(X, t)$  for  
92 different  $R_0$  are controlled solely by the rescaled time  
93  $\tau := v_\infty t / R_0$ , as follows: statistical properties of  $\chi(X, t)$   
94 agree with those for the *flat* subclass initially ( $\tau \ll 1$ ),  
95 until the interfaces nearly collapse at  $\tau \approx 1$  and therefore  
96 do not behave as KPZ anymore. Analogous behavior was  
97 also observed numerically by Carrasco and Oliveira [27],  
98 who used lattice models with system size set to decrease  
99 in time (mimicking the shrinking circumference of the  
100 ingrowing interfaces). The case of enlarging substrates,  
101 which would correspond to the outgrowing case, has also  
102 been studied and crossover from the flat to circular sub-  
103 classes was suggested in this case [27–29], which is also  
104 expected to be described by  $\tau$ . However, it remains un-  
105 clear how universal such finite-time behavior is, why  $\tau$   
106 is the right parameter to describe it, and above all, how  
107 such crossover can be described theoretically.

108 Those problems are addressed and answered in this  
109 Letter. We study outgrowing interfaces from ring initial  
110 conditions both numerically and experimentally, using an  
111 off-lattice version of the Eden model [30] and the liquid-  
112 crystal turbulence [4, 10–12]. Scaling functions for the  
113 flat-to-circular crossover are determined, and shown to  
114 be the same for both of the studied systems. Moreover,  
115 we describe this crossover theoretically, by adapting the  
116 variational formula [16, 23–26] for curved initial condi-  
117 tions. The formula is numerically evaluated and shown to  
118 reproduce our numerical and experimental results quan-  
119 titatively, without adjustable parameters. This also im-  
120 plies that the flat-to-circular crossover is indeed universal  
121 and, furthermore, should generally appear for *any* curved  
122 interfaces with locally parabolic initial conditions.

123 We first study the off-lattice Eden model [30], in which  
124 a cluster of round particles (with unit diameter) grows  
125 by stochastic addition of new particles. The initial con-  
126 dition is set to be a ring of  $N$  particles [Fig. 1(a)].  
127 The evolution rule is as follows (see Ref. [30] for de-  
128 tails): at each time step, we randomly choose a par-  
129 ticle at the interface, attempt to put a new particle  
130 next to it in a random direction and do so if there  
131 is no overlapping particle. Time is then increased by

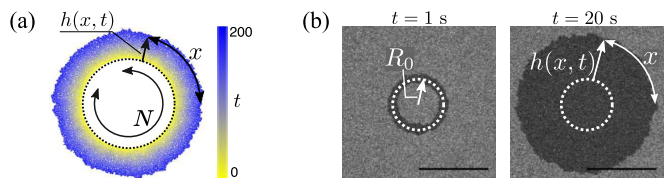


FIG. 1. Typical snapshots from the Eden simulations and the liquid-crystal experiments. (a) An Eden interface growing outward from a ring with  $N = 1000$  (dotted line). Time is indicated by the color. (b) A DSM2 cluster (black) growing from a ring with  $R_0 = 366 \mu\text{m}$  (dotted lines). The elapsed time after shooting laser is indicated above each image. The scale bar corresponds to 1 mm.

132  $1/(\text{the number of the interfacial particles})$  whether the  
133 new particle was put or not. Particles that cannot con-  
134 tribute further growth were checked and removed from  
135 the list of the interfacial particles every time unit. To  
136 characterize the height fluctuations, we measure the lo-  
137 cal radius increment  $R(\theta, t)$ , which is the radial distance  
138 between the initial ring and the interface at each angular  
139 position  $\theta$  [Fig. 1(a)]. Thanks to the rotational symme-  
140 try, we have

$$R(\theta, t) \stackrel{\text{d}}{=} h(0, t) \simeq v_\infty t + (\Gamma t)^{1/3} \chi(0, t), \quad (3)$$

141 but statistical precision can be improved by averaging  
142 over  $\theta$ . In our simulations, we varied the initial size  $N$   
143 from 100 to 40000 and obtained 4320 to 14400 realiza-  
144 tions for each case (summarized in Table SI [31]). For  
145 comparison, we also simulated flat interfaces, for which  
146 the initial condition was a line formed by 75000 parti-  
147 cles and the periodic boundary condition in the spanwise  
148 direction was used, and obtained 14400 realizations.

149 To characterize statistical properties of the stochas-  
150 tic variable  $\chi(X, t)$ , we first estimated the non-universal  
151 parameters  $v_\infty, \Gamma$  and  $A$ , from the data for the flat inter-  
152 faces.  $v_\infty$  and  $\Gamma$  were obtained by the standard procedure  
153 [4], specifically by using  $\partial_t \langle h \rangle \simeq v_\infty + \text{const.} \times t^{-2/3}$  and  
154  $\langle h^2 \rangle_c / (t^{2/3} \langle \chi_1^2 \rangle_c) \simeq \Gamma^{2/3}$ , where  $\langle \dots \rangle_c$  denotes the  
155  $k$ th-order cumulant and here we used the fact that the  
156 asymptotic fluctuations of the flat interfaces are given  
157 by the GOE Tracy-Widom distribution. We obtained  
158  $v_\infty = 0.51370(5)$  and  $\Gamma = 0.980(3)$ . The parameter  $A$   
159 was obtained by  $A = \sqrt{2\Gamma/v_\infty}$ , the relationship valid for  
160 isotropic growth [11].

161 With those parameter values, we define the rescaled  
162 height

$$q(\theta, t) := \frac{R(\theta, t) - v_\infty t}{(\Gamma t)^{1/3}} \stackrel{\text{d}}{\simeq} \chi(0, t) \quad (4)$$

163 and measure its mean and variance as functions of time,  
164 for different initial particle number  $N$  (Fig. 2 left). Fig-

Figure 2 also shows the rescaled mean velocity [4, 12]

$$\begin{aligned} \langle p(\theta, t) \rangle &:= \left\langle \frac{3t^{2/3}}{\Gamma^{1/3}} [\partial_t R(\theta, t) - v_\infty] \right\rangle \\ &\simeq \langle \chi(0, t) \rangle + 3t \partial_t \langle \chi(0, t) \rangle, \end{aligned} \quad (5)$$

which asymptotically goes to  $\langle \chi(0, t) \rangle$  if  $\langle \chi(0, t) \rangle$  converges sufficiently fast. For the flat case (gray circles),  $\langle q \rangle \rightarrow \langle \chi_1 \rangle$ ,  $\langle p \rangle \rightarrow \langle \chi_1 \rangle$  and  $\langle q^2 \rangle_c \rightarrow \langle \chi_1^2 \rangle_c$  as expected. In the case of the ring initial conditions, for large  $N$  the data first behave similarly to the flat case, then deviate and approach the values for the circular subclass,  $\langle \chi_2 \rangle$  and  $\langle \chi_2^2 \rangle_c$  [32]. This crossover takes place earlier for smaller  $N$ . Indeed, when the data are plotted against the rescaled time  $\tau = v_\infty t / R_0$  ( $R_0 = N/2\pi$ ), all data collapse onto a single curve except for the non-universal short-time regime (Fig. 2 right). This suggests that the distribution of  $\chi(0, t)$  for different  $R_0$ , denoted by  $\chi(0, t; R_0)$ , is described by a single stochastic variable  $\chi_c(0, \tau)$ , parametrized by  $\tau$ , as follows:

$$\chi(0, t; R_0) \stackrel{d}{\rightarrow} \chi_c(0, \tau), \quad (R_0, t \rightarrow \infty) \quad (6)$$

where the double limit is taken with fixed  $\tau = v_\infty t / R_0$ . Then the flat-to-circular crossover we found indicates  $\chi_c(0, \tau) \stackrel{d}{\rightarrow} \chi_1$  for  $\tau \rightarrow 0$  and  $\chi_c(0, \tau) \stackrel{d}{\rightarrow} \chi_2$  for  $\tau \rightarrow \infty$ . The skewness  $\text{Sk}[R(\theta, t)] := \langle R^3 \rangle_c / \langle R^2 \rangle_c^{3/2} \rightarrow \text{Sk}[\chi_c(0, \tau)]$  and the kurtosis  $\text{Ku}[R(\theta, t)] := \langle R^4 \rangle_c / \langle R^2 \rangle_c^2 \rightarrow \text{Ku}[\chi_c(0, \tau)]$  show consistent behavior (Fig. S1 [31]).

We also study this crossover in the spatial correlation. In the case of the point initial condition, suppose  $\theta = 0$  corresponds to  $x = 0$ , then using  $R(\theta, t) = \sqrt{h(x, t)^2 + x^2} \simeq h + \frac{x^2}{2h}$  and Eq. (2), we can show  $q(\theta, t) \stackrel{d}{\rightarrow} \mathcal{A}_2(X)$ . Therefore, the rescaled spatial covariance  $C_s(\Delta X, t) := \langle q(\theta + \Delta\theta, t)q(\theta, t) \rangle - \langle q(\theta, t) \rangle^2$  with  $\Delta X := \langle R(\theta, t) \Delta\theta / \xi(t) \rangle$  can be directly compared with the covariance of the Airy<sub>1</sub> and Airy<sub>2</sub> processes. Our numerical results for the ring initial conditions (Fig. S2 filled symbols) indeed show crossover from the Airy<sub>1</sub> covariance ( $\tau \ll 1$ ) to the Airy<sub>2</sub> covariance ( $\tau \gg 1$ ), consistently to the results on the one-point distribution.

To test universality of our finding, in particular the function forms of  $\langle \chi_c(0, \tau) \rangle$  and  $\langle \chi_c(0, \tau)^2 \rangle_c$ , we conducted experiments on liquid-crystal turbulence [4, 10–12]. As in the previous studies, we applied an AC voltage (here, 22 V at 300 Hz) to nematic liquid crystal filling a thin gap between transparent electrodes, and observed growth of a turbulent state called the dynamic scattering mode 2 (DSM2), expanding in a metastable turbulent state, DSM1 (see Supplemental Text [31] for detailed methods). DSM2 was generated by emitting a few ultraviolet laser pulses [4]. Using the holographic technique we previously adopted for the DSM2 growth experiments [12], we formed the laser intensity profile in the shape of

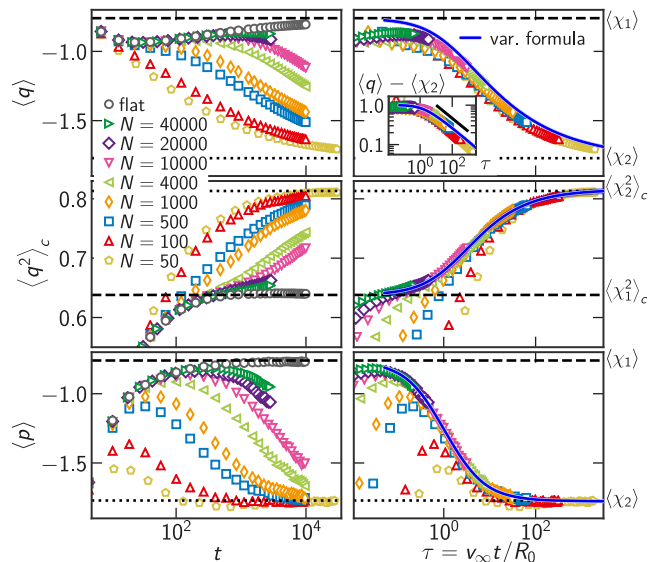


FIG. 2. The mean and variance of the rescaled height,  $\langle q(\theta, t) \rangle$  and  $\langle q(\theta, t)^2 \rangle_c$ , and the rescaled mean velocity  $\langle p(\theta, t) \rangle$  for the Eden model in the outgrowing case. The data are shown against the raw time  $t$  (left) and the rescaled time  $\tau = v_\infty t / R_0$  (right). The theoretical curves evaluated numerically from the variational formula for the outgrowing interfaces (=var., blue solid line) are shown in the right panels. The values of  $\chi_1$  and  $\chi_2$  are shown by the dashed and dotted lines, respectively. The inset of the right-top figure shows the difference between the data and the expected long-time limit value,  $\langle \chi_2 \rangle$ . The black solid line indicates slope  $-1/3$ .

a ring of a given radius  $R_0$ , which sets the initial condition of the DSM2 interface [Fig. 1(b)]. We also generated circular interfaces with a point initial condition, and flat interfaces with a linear initial condition. We obtained 941 to 1936 realizations for each case (Table SII [31]), recorded by a charge-coupled device camera. The radius  $R(\theta, t)$  of the DSM2 interfaces (or the height  $h(x, t)$  for the flat case) was determined from each image, with the time  $t$  defined as the elapsed time after shooting the laser pulses. Then the non-universal parameters  $v_\infty, \Gamma, A$  were evaluated in the same way as for the Eden model, here for the flat and point initial conditions (Table SII [31]). Although the values of  $v_\infty, \Gamma, A$  are expected to be independent of the initial condition, in practice one needs to evaluate for each set of experiments, because of unavoidable slight changes in experimental conditions [11]. For the ring initial conditions, however, the parameter values could not be obtained in the same way because of the time dependence (i.e., crossover) of  $\chi(X, t)$ . We therefore used the values obtained from the flat case for the outgrowing cases, unless otherwise stipulated. Possible shifts in the parameter values were taken into account in the uncertainty estimates for the outgrowing cases, evaluated from the differences in the parameter values between the flat and circular cases.

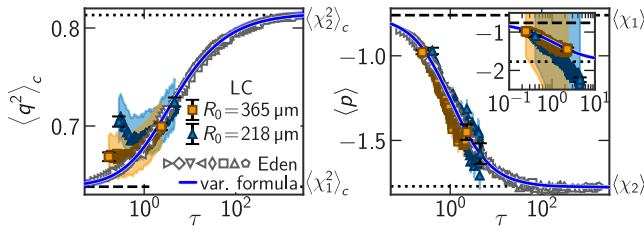


FIG. 3. Comparison of the results from the experiments (color filled symbols), the Eden simulations (gray open symbols), and the variational formula (=var., blue solid line), for the outgrowing interfaces. The variance of the rescaled height,  $\langle q(\theta, t)^2 \rangle_c$ , and the rescaled mean velocity  $\langle p(\theta, t) \rangle$  are shown in the left and right panels, respectively, against  $\tau = v_\infty t / R_0$ . For the numerical results, data with  $t > 10^3$  are shown by the same symbols as those in Fig. 2. For the experimental results, statistical errors are indicated by the error bars on the first and last data points, and uncertainty associated with the parameter estimation is shown by the shaded areas. The values for  $\chi_1$  (flat) and  $\chi_2$  (circular) are shown by the dashed and dotted lines, respectively. The inset of the right panel shows the experimental results obtained with  $v_\infty$  from the flat case, while it was adjusted in the main panel to fit the Eden data at the largest  $t$  (see text).

Now we compare the experimental results with those for the Eden model. Figure 3 left panel shows the variance of the rescaled height,  $\langle q(\theta, t)^2 \rangle_c$ , against  $\tau = v_\infty t / R_0$ , which overlaps on the Eden data within statistical errors and parameter uncertainty (error bars and shades, respectively) apart from the non-universal short-time behavior. For the rescaled mean velocity  $\langle p(\theta, t) \rangle$  (right panel), the uncertainty of  $v_\infty$  was too large to make a meaningful comparison (inset). However, if we instead choose the value of  $v_\infty$  in such a way that  $\langle p(\theta, t) \rangle$  at the largest  $t$  falls onto the curve for the Eden model (obtained values of  $v_\infty$  are given in Table SII),  $\langle p(\theta, t) \rangle$  overlaps for all  $t$  (main panel). Those results of  $\langle q(\theta, t)^2 \rangle_c$  and  $\langle p(\theta, t) \rangle$  suggest universality of the one-point distribution of  $\chi_c(0, \tau)$ . Moreover, the spatial covariance  $C_s(\Delta X, t)$  is also found to overlap with the results of the Eden model if the value of  $\tau$  is close enough (Fig. S2). This suggests that not only the one-point distribution of  $\chi_c(0, \tau)$  but the spatial covariance of  $\chi_c(X, \tau)$  is also universal.

So far we have characterized the flat-to-circular crossover and found it to be controlled by a single parameter  $\tau = v_\infty t / R_0$ , but why so and how can this crossover be theoretically described? To answer these questions, we employ the variational formula [16, 23–26] and apply it to a general, curved initial condition.

The variational formula describes the height  $h(x, t)$  for a general initial condition  $h(x, 0) =: h_0(x)$  as follows

$$h(x, t) \stackrel{\text{d}}{\simeq} \sup_{y \in \mathbb{R}} [h_{\text{circ}}(x, t; y) + h_0(y)], \quad (7)$$

where  $h_{\text{circ}}(x, t; y)$  denotes the height for the point initial condition nucleating at position  $y$ , growing with the

same realization of noise for different  $y$  [23]. Intuitively, this means that the initial condition  $h(x, 0)$  can be regarded as a collection of point sources and  $h(x, t)$  is then given by the envelope of the circular interfaces from those point sources, a bit analogously to Huygens' principle [33]. The formula (7) involves a mathematical object called the Airy sheet [23, 25], but if the interest is only in the one-point distribution, it can be simply expressed by the  $\text{Airy}_2$  process, as follows [16, 24]:

$$\chi(X, t) \stackrel{\text{d}}{\simeq} \sup_{Y \in \mathbb{R}} \left[ \mathcal{A}_2(X - Y) - (X - Y)^2 + \frac{h_0(\xi(t)Y)}{(\Gamma t)^{1/3}} \right]. \quad (8)$$

We use Eq. (8) and consider a class of curved initial conditions in the following form

$$h_0(x) = R_0 g\left(\frac{x}{R_0}\right) \quad (9)$$

where  $g(w)$  is a locally parabolic function, i.e.,  $g(w) = -c_2 w^2 + \mathcal{O}(w^2)$  for small  $|w|$ . Substituting Eq. (9) into Eq. (8), taking the limit  $R_0, t \rightarrow \infty$  with fixed  $\tau = v_\infty t / R_0$ , and setting  $x = 0$  yields

$$\chi(0, t) \stackrel{\text{d}}{\simeq} \sup_{Y \in \mathbb{R}} [\mathcal{A}_2(Y) - (1 + c\tau)Y^2] =: \tilde{\chi}(c\tau) \quad (10)$$

with  $c := (4c_2\Gamma)/(A^2v_\infty)$ . This shows that the asymptotic height distribution is parameterized only by  $c\tau$ , and only the local functional form of  $g(w)$  at small  $|w|$  is relevant. The characteristic time is  $\tau = 1/c$  and therefore  $t = A^2R_0/4c_2\Gamma$ , and this is the time at which the initial height difference  $|h_0(0) - h_0(\xi(t))|$  becomes comparable to the fluctuation amplitude,  $(\Gamma t)^{1/3}$ . For isotropic growth, the relationship  $A = \sqrt{2\Gamma/v_\infty}$  [11] further yields  $c = 2c_2$ .

For the ring initial conditions,  $g(w)$  is given by  $g(w) = \sigma(\sqrt{1-w^2}\mathbb{1}_{|w|<1} - 1)$  with  $\sigma = +1$  ( $-1$ ) for the outgrowing (ingrowing) case. Then we obtain  $\chi(0, t) \stackrel{\text{d}}{\simeq} \tilde{\chi}(\sigma\tau)$ , which we have expressed by  $\chi_c(0, \tau)$  for the outgrowing case  $\sigma = +1$  [Eq. (6)]. Note that, mathematically, it is known that  $\tilde{\chi}(0) = \sup_{Y \in \mathbb{R}} (\mathcal{A}_2(Y) - Y^2) \stackrel{\text{d}}{=} \chi_1$ , i.e., GOE Tracy-Widom distribution [34, 35]. In the other limit  $\tau \rightarrow \infty$ , clearly,  $\tilde{\chi}(\tau) \rightarrow \mathcal{A}_2(0) \stackrel{\text{d}}{=} \chi_2$ , i.e., GUE Tracy-Widom distribution. Therefore,  $\chi_c(0, \tau) = \tilde{\chi}(\tau)$  indeed has the expected limits on both sides of the flat-to-circular crossover.

To compare the variational formula with the experimental and numerical data for finite  $\tau$ , we employ a Monte Carlo method to evaluate Eq. (10). The  $\text{Airy}_2$  process  $\mathcal{A}_2(Y)$  is in fact known to be equivalent to the largest eigenvalue of large GUE random matrices undergoing Dyson's Brownian motion [16, 34]. We therefore implement Dyson's Brownian motion numerically, in the form of the Ornstein-Uhlenbeck process of Hermitian random matrices and obtained approximated realizations of



$\mathcal{A}_2(Y)$  (see Supplemental Text [31] for details). Then we evaluated the supremum of Eq. (10), interpolating the values of  $\mathcal{A}_2(Y)$  between the discrete steps by using the Brownian bridge [31]. The results for the outgrowing case ( $\sigma = +1$ ) are shown in Figs. 2 and 3, where the data of the mean  $\langle q \rangle$ , variance  $\langle q^2 \rangle_c$ , and the rescaled mean velocity  $\langle p \rangle$  are compared with the corresponding expressions of  $\tilde{\chi}(\tau)$ , specifically,  $\langle \tilde{\chi}(\tau) \rangle$ ,  $\langle \tilde{\chi}(\tau)^2 \rangle_c$  [Eq. (4)], and  $\langle \tilde{\chi}(\tau) \rangle + 3\tau\partial_\tau \langle \tilde{\chi}(\tau) \rangle$  [Eq. (5)], respectively. The results of the variational formula precisely agree, without any adjustable parameter, with the numerical and experimental data. We also inspected the ingrowing case  $\sigma = -1$  and confirmed the validity of the variational formula (Fig. S3). The agreement was also underpinned for the skewness and kurtosis (Fig. S4).

In summary, we found KPZ crossover functions that govern height fluctuations of interfaces growing outward from ring initial conditions, parameterized only by the rescaled time  $\tau = v_\infty t/R_0$ , and evidenced their universality both experimentally and numerically. We then presented a theoretical description of this crossover, on the basis of the KPZ variational formula for general curved initial conditions. We numerically evaluated the formula and found remarkable agreement with the experimental and numerical data. Our results constitute the first example where the KPZ variational formula was successfully used to describe experimental observations, showing the ability of this formula to explain, or even predict, real data from general initial conditions. We hope our work will trigger further studies to elucidate geometry-dependent universality of the KPZ class and beyond.

We thank P. Le Doussal for useful discussions on the variational formula, and F. Bornemann for the theoretical curves of the  $\text{Airy}_1$  and  $\text{Airy}_2$  covariance [36]. We thank Supercomputer Center of the Institute for Solid State Physics (the University of Tokyo) and Meiji Institute for Advanced Study of Mathematical Sciences (Meiji University) for computational facilities. We acknowledge financial support by KAKENHI from Japan Society for the Promotion of Science (Grant Nos. JP25103004, JP16H04033, JP19H05800, JP19H05144, JP17J05559), by Yamada Science Foundation, and by the National Science Foundation (Grant No. NSF PHY11-25915).

\* ysk@yfukai.net

† kat@kaztake.org

- [1] M. Kardar, G. Parisi, and Y.-C. Zhang, Phys. Rev. Lett. **56**, 889 (1986).  
 [2] A.-L. Barabási and H. Eugene Stanley, *Fractal Concepts in Surface Growth* (Cambridge University Press, New York, NY, USA, 1995).  
 [3] For recent reviews, see, e.g., T. Kriecherbauer and J. Krug, J. Phys. A: Math. Theor. **43**, 403001 (2010); I. Corwin, Random Matrices Theory Appl. **01**, 1130001

- (2012); J. Quastel and H. Spohn, J. Stat. Phys. **160**, 965 (2015); T. Halpin-Healy and K. A. Takeuchi, J. Stat. Phys. **160**, 794 (2015); T. Sasamoto, Prog. Theor. Exp. Phys. **2016**, 022A01 (2016).  
 [4] For lecture notes, see: K. A. Takeuchi, Physica A **504**, 77 (2018).  
 [5] H. Spohn, in *Thermal Transport in Low Dimensions*, Lecture Notes in Physics No. 921 (Springer International Publishing, 2016) pp. 107–158.  
 [6] K. A. Takeuchi, J. Stat. Mech. Theor. Exp. **2014**, P01006 (2014).  
 [7] J.-i. Wakita, H. Itoh, T. Matsuyama, and M. Matsushita, J. Phys. Soc. Jpn. **66**, 67 (1997).  
 [8] M. A. C. Huergo, M. A. Pasquale, A. E. Bolzán, A. J. Arvia, and P. H. González, Phys. Rev. E **82**, 031903 (2010); M. A. C. Huergo, M. A. Pasquale, P. H. González, A. E. Bolzán, and A. J. Arvia, Phys. Rev. E **84**, 021917 (2011); Phys. Rev. E **85**, 011918 (2012).  
 [9] J. Maunuksela, M. Myllys, O.-P. Kähkönen, J. Timonen, N. Provatas, M. J. Alava, and T. Ala-Nissila, Phys. Rev. Lett. **79**, 1515 (1997).  
 [10] K. A. Takeuchi and M. Sano, Phys. Rev. Lett. **104**, 230601 (2010); K. A. Takeuchi, M. Sano, T. Sasamoto, and H. Spohn, Sci. Rep. **1**, 34 (2011).  
 [11] K. A. Takeuchi and M. Sano, J. Stat. Phys. **147**, 853 (2012).  
 [12] Y. T. Fukai and K. A. Takeuchi, Phys. Rev. Lett. **119**, 030602 (2017).  
 [13] T. Sasamoto, J. Phys. A: Math. Gen. **38**, L549 (2005).  
 [14] A. Borodin, P. L. Ferrari, M. Prähofer, and T. Sasamoto, J. Stat. Phys. **129**, 1055 (2007).  
 [15] M. Prähofer and H. Spohn, J. Stat. Phys. **108**, 1071 (2002).  
 [16] J. Quastel and D. Remenik, in *Topics in Percolative and Disordered Systems* (Springer, New York, NY, 2014) pp. 121–171.  
 [17] J. Baik, P. Deift, and K. Johansson, J. Amer. Math. Soc. **12**, 1119 (1999).  
 [18] K. Johansson, Commun. Math. Phys. **209**, 437 (2000).  
 [19] J. Baik and E. M. Rains, in *Random Matrix Models and Their Applications*, MSRI Publications, Vol. 40, edited by P. Bleher and A. Its (Cambridge Univ. Press, Cambridge, 2001) pp. 1–19, arXiv:math/9910019.  
 [20] M. Prähofer and H. Spohn, Physica A **279**, 342 (2000); M. Prähofer and H. Spohn, Phys. Rev. Lett. **84**, 4882 (2000).  
 [21] C. A. Tracy and H. Widom, Commun. Math. Phys. **159**, 151 (1994); Commun. Math. Phys. **177**, 727 (1996).  
 [22] G. W. Anderson, A. Guionnet, and O. Zeitouni, *An Introduction to Random Matrices*, 118 (Cambridge University Press, 2010).  
 [23] I. Corwin, J. Quastel, and D. Remenik, J. Stat. Phys. **160**, 815 (2015).  
 [24] I. Corwin, Z. Liu, and D. Wang, Ann. Appl. Probab. **26**, 2030 (2016).  
 [25] D. Dauvergne, J. Ortman, and B. Virág, (2019), arXiv:1812.00309.  
 [26] J. Quastel and D. Remenik, Trans. Amer. Math. Soc. **371**, 6047 (2019).  
 [27] I. S. S. Carrasco and T. J. Oliveira, Phys. Rev. E **98**, 010102(R) (2018).  
 [28] I. S. S. Carrasco, K. A. Takeuchi, S. C. Ferreira, and T. J. Oliveira, New J. Phys. **16**, 123057 (2014).  
 [29] I. S. S. Carrasco and T. J. Oliveira, Phys. Rev. E **99**,

- 427 032140 (2019).  
 428 [30] K. A. Takeuchi, J. Stat. Mech. Theor. Exp. **2012**, P05007  
 429 (2012).  
 430 [31] See Supplemental Material for the detailed experimental  
 431 methods, numerical evaluation of the variational formula,  
 432 Tables SI and SII and Figs. S1, S2, S3, S4 and S5, which  
 433 includes Refs. [37–41].  
 434 [32] Though the value of  $\langle q \rangle$  does not fully converge to  $\langle \chi_2 \rangle$   
 435 even at the largest  $\tau$  we reached, the difference seems  
 436 to converge to zero with a power law with an exponent  
 437 close to  $-1/3$  (inset of Fig. 2). This suggests convergence  
 438 of  $\langle q \rangle$  to  $\langle \chi_2 \rangle$  in the limit of  $t \rightarrow \infty$ .  
 439 [33] Though nonlinear equations generally do not admit the  
 440 principle of superposition, the KPZ equation can be  
 441 mapped to a linear equation by the Cole-Hopf transfor-  
 442 mation and this leads to the variational formula (7) [16].  
 443 [34] K. Johansson, Commun. Math. Phys. **242**, 277 (2003).  
 444 [35] I. Corwin, J. Quastel, and D. Remenik, Commun. Math.  
 445 Phys. **317**, 347 (2013).  
 446 [36] F. Bornemann, Math. Comput. **79**, 871 (2010).  
 447 [37] P. G. de Gennes and J. Prost, *The Physics of Liq-*  
 448 *uid Crystals* (Oxford University Press, U.S.A., Oxford,  
 449 1995).  
 450 [38] D. T. Gillespie, Phys. Rev. E **54**, 2084 (1996).  
 451 [39] J. Hägg, Ann. Probab. **36**, 1059 (2008).  
 452 [40] L. Beghin and E. Orsingher, Lith. Math. J. **39**, 157  
 453 (1999).  
 454 [41] I. M. Johnstone and Z. Ma, Ann. Appl. Probab. **22**, 1962  
 455 (2012).